

Article

Local Energy Velocity of the Air-Core Modes in Hollow-Core Fibers

Andrey Pryamikov 

Prokhorov General Physics Institute of the Russian Academy of Sciences, 119991 Moscow, Russia; pryamikov@mail.ru

Abstract: In this paper, we consider the behavior of the local energy flow velocity of the fundamental air-core mode at the core-cladding boundary in two types of hollow-core fibers: hollow-core fibers with a negative curvature of the core boundary and single-capillary fibers with similar geometrical parameters. It is demonstrated that the behavior of both axial and radial components of the local energy velocity of the fundamental air-core mode is completely different for these two types of hollow-core fibers. The negative curvature of the core boundary leads to an alternating behavior of the radial projection of the local energy velocity and a decrease of two orders of magnitude compared to the values of this projection for a single capillary. In our opinion, this behavior of the local energy velocity of the fundamental air-core mode is caused by a periodic set of Poynting vector vortices that appear in the cladding capillary walls.

Keywords: local energy velocity; vortex; Poynting vector; air-core modes; hollow-core fibers; losses

1. Introduction

The development of hollow-core fibers for transmitting radiation over long distances began with work [1], in which the optical properties of a waveguide in the form of a tube in an infinite dielectric medium or metal were considered. For such a hollow-core dielectric waveguide made of glass with a refractive index $n = 1.5$ and a hollow-core radius $R = 1$ mm, a loss of 1.85 dB/km was predicted at a wavelength of 1 μm for the EH_{11} hybrid mode. In this case, the main problem turned out to be bending losses, the level of which did not allow the use of such hollow-core waveguides in practice. It was necessary to reduce the radius of the hollow core and complicate the structure of the cladding of the hollow-core fiber. A breakthrough solution to this problem was the creation of hollow-core microstructured fibers [2]. The minimum losses achieved in hollow-core photonic crystal fibers were at the level of 1.2 dB/km at a wavelength of 1.55 μm , and their further reduction was limited by scattering due to surface roughness from frozen surface capillary waves [3]. Light localization in hollow-core photonic crystal fibers occurs due to the formation of photonic band gaps. Further development of hollow-core fibers and their applications in the field of telecommunications is associated with the creation of hollow fibers with negative curvature of the core-cladding boundary [4–6]. The mechanism of light localization in hollow-core fibers with a negative curvature of the core-cladding boundary has been investigated for over ten years. The importance of understanding the mechanism of light localization in these fibers lies in the fact that, at the moment, in modified fibers of this type (nested hollow-core fibers), losses of 0.174 dB/km have already been achieved in the telecommunications C-band [7]. By now, several models have been proposed to explain strong light localization in the air core, which enables radiation transmission at high losses of the fiber material [8] and high-power radiation [9]. In this paper, we will examine the problem of light localization from a slightly different angle, which could give impetus to a new understanding of the processes in hollow-core fibers with a rather simple design.

To date, the ARROW (Anti-Resonant Reflective Optical Waveguide) model is considered to be the main model by most authors working in this field [10,11]. According



Citation: Pryamikov, A. Local Energy Velocity of the Air-Core Modes in Hollow-Core Fibers. *Photonics* **2023**, *10*, 1035. <https://doi.org/10.3390/photonics10091035>

Received: 17 August 2023

Revised: 1 September 2023

Accepted: 8 September 2023

Published: 10 September 2023



Copyright: © 2023 by the author. Licensee MDPI, Basel, Switzerland. This article is an open access article distributed under the terms and conditions of the Creative Commons Attribution (CC BY) license (<https://creativecommons.org/licenses/by/4.0/>).

to this model, each element of the cladding of a microstructured fiber can be considered an analog of a Fabry–Perrot resonator. Therefore, at certain wavelengths, these elements either effectively reflect radiation into the core of the fiber, localizing the radiation in an antiresonant regime, or effectively transmit radiation into the surrounding space, which leads to large losses. This model was originally developed to explain the appearance of transmission bands and low losses in planar waveguides and was then transferred to the field of micro-structured fibers to explain light localization in them. From the point of view of calculating transmission band edges, this model yields good results that closely correspond to experimental data. Yet, if we consider the mechanism of low-loss formation in the centers of the transmission bands of the hollow-core fibers, there are facts that do not allow us to interpret the cladding capillary walls of the hollow-core fibers simply as planar Fabry-Perrot resonators. Therefore, there have appeared several alternative views on this problem, such as the inhibited coupling model [12], vortex-supported waveguiding model [13], and azimuthal confinement model [14].

In this work, we propose to introduce a concept of the local energy velocity of air-core modes and, on its basis, to compare mechanisms of energy leakage from a silica glass capillary and silica glass hollow-core fibers with a cladding consisting of capillaries (a negative curvature of the core-cladding boundary). While in the former case we obtained the expected results for the local energy velocity at the inner capillary boundary, in the latter case we obtained a more interesting and complex picture of the air-core mode energy leakage process at the outer boundary of cladding capillaries. Firstly, in some areas of the cladding capillary boundary, the local energy velocity drops by four orders of magnitude in the radial direction compared to the speed of light in a vacuum. In addition, in these regions, the behavior of the local energy velocity of the fundamental air-core mode also changes along the fiber axis. These phenomena were earlier observed in planar waveguide structures made of left-handed metamaterials and epsilon-negative materials (sandwich structures consisting of epsilon-negative/left-handed/epsilon negative metamaterials) [15,16]. They are associated with radiation power flows moving in opposite directions along the boundaries of such planar waveguide structures and emerging vortices of electromagnetic fields and power flows at these boundaries. As a result, the power flows between two metamaterials cancel each other out, and the total power flow tends to be zero. We demonstrate that this phenomenon can also occur in the cladding of hollow-core fibers with a negative curvature of the core-cladding boundary. The proposed approach makes it possible to analyze the behavior of the energy fluxes of the core modes of fibers with a complex cladding structure that does not have translational symmetry.

The paper is structured as follows: the first part examines the behavior of the local energy velocity in a single silica glass capillary; the second part analyzes the distribution of the local energy velocity at the outer boundaries of the cladding capillaries of hollow-core fibers with one layer of capillaries in the cladding and nested hollow-core fiber; and the final part contains a discussion of the findings.

2. Local Energy Velocity of the Fundamental Air-Core Mode for a Silica Glass Capillary

In this section, we analyze the behavior of the local energy velocity of the fundamental air-core mode in different regions of the cross-section of a silica glass capillary. Let us consider a capillary with an air-core diameter of $D_{core} = 50 \mu\text{m}$ and a wall thickness of $t = 750 \text{ nm}$, which, according to the ARROW model [10], approximately corresponds to the center of the second transmission band at a wavelength of $\lambda = 1.06 \mu\text{m}$. According to the waveguide theory, the electric and magnetic fields of the fundamental air-core mode (HE_{11} hybrid mode) can be represented in cylindrical coordinates (r, φ, z) as:

$$E_z = AF(k_t r) \cos \varphi,$$

$$H_z = BF(k_t r) \sin \varphi,$$

$$\begin{aligned}
 E_r &= \frac{-i}{k_t^2} \left[A\beta k_t F'(k_t r) + B\omega\mu_0 \frac{1}{r} F(k_t r) \right] \cos \varphi, \\
 E_\varphi &= \frac{-i}{k_t^2} \left[A\beta \frac{1}{r} F(k_t r) + B\omega\mu_0 k_t F'(k_t r) \right] \sin \varphi, \\
 H_r &= \frac{-i}{k_t^2} \left[A\omega\varepsilon_0 n_i^2 \frac{1}{r} F(k_t r) + B\beta k_t F'(k_t r) \right] \sin \varphi, \\
 H_\varphi &= \frac{-i}{k_t^2} \left[A\omega\varepsilon_0 n_1^2 F'(k_t r) + B\beta \frac{1}{r} F(k_t r) \right] \cos \varphi,
 \end{aligned}
 \tag{1}$$

where in (1) the dependence on time and axial coordinates in the form of $e^{i(\omega t - \beta z)}$ is omitted. In Formula (1), the following notations are introduced: $k_t = \sqrt{n_i^2 \omega^2 / c^2 - \beta^2}$, where n_i ($i = 1, 2$) are refractive indices of air and glass in the capillary cross-section, ω is circular frequency and $\beta = n_{eff} \omega / c$, where n_{eff} is an effective refractive index of the fundamental air-core mode and c is the speed of light. Function $F(k_t r)$ is the Bessel function of the first kind $J_1(k_t r)$ in the capillary core, the sum of two Hankel functions $H_1^{(1)}(k_t r) + H_1^{(2)}(k_t r)$ in the capillary wall, and simply the Hankel function $H_1^{(2)}(k_t r)$ outside the capillary. A and B are amplitude coefficients.

Based on Formula (1), it is possible to calculate the power flux and the energy density of the fundamental air-core mode averaged over the oscillation period. The formulas for them are as follows:

$$\begin{aligned}
 \vec{P} &= \frac{1}{2} \text{Re} \left(\vec{E} \times \vec{H}^* \right), \\
 W &= \frac{1}{4} \left(\varepsilon |\vec{E}|^2 + \mu |\vec{H}|^2 \right),
 \end{aligned}
 \tag{2}$$

Knowing these two quantities, one can calculate a local value characterizing the rate and direction of the air-core mode energy flow in the vicinity of certain points of the capillary cross-section. This value has a similar expression as the value of the energy velocity of the plane wave [17]:

$$\vec{V}(r, \varphi) = \frac{\vec{P}}{W}.
 \tag{3}$$

It can be seen from (3) that \vec{V} does not depend on the z -coordinate since the power flow and energy density have the same dependence on the axial coordinate in the form of $e^{-2\text{Im}(\beta)z}$. As it will be seen below, the study of the distribution of the local energy velocity of the air-core modes can be specifically useful for fibers with a complex shape of the core-cladding boundary. In our previous papers [13,18–20], we considered in sufficient detail the behavior of energy fluxes and streamlines of the Poynting vector of core modes for various micro-structured fibers, including those with a complex shape of the core-cladding boundary.

In the case of a simple waveguide, which is a silica glass capillary, this value along its inner boundary has a simple distribution that can be easily calculated using Formulas (1)–(3). All terms in expressions for \vec{P} and W (2) of the $E_r H_\varphi^*, E_\varphi H_r^*, E_r E_r^*, H_\varphi H_\varphi^*$ etc. type have an angular dependence of $\cos^2 \varphi$. It is clear that all terms obtained by multiplying projections of the electric and magnetic fields of the fundamental air-core mode in (2) can be functions of either the radial coordinate or have an azimuthal angle dependence in the form of $\cos 2\varphi$. In general, the dependences on the azimuthal angle for the projections of \vec{P} and the mode energy density W can be expressed as:

$$P_j(r, \varphi) = C_1 F_1(r) + C_2 F_2(r) \cos(2\varphi),
 \tag{4}$$

$$W(r, \varphi) = D_1 G_1(r) + D_2 G_2(r) \cos(2\varphi),$$

where $j = (x, y, z)$, C_i, D_i are constants obtained by multiplying expressions (1) while $F_i(r)$ and $G_i(r)$ are functions of the radial coordinate ($i = 1, 2$). The calculated distributions for the axial P_z/W and radial P_r/W projections of \vec{V} along the inner boundary of the capillary described at the beginning of this section are shown in Figure 1. These distributions confirm the dependence on the azimuthal angle in the form of (4). The values of the projections of V_z are positive along the entire inner boundary of the capillary and have values that are approximately an order of magnitude less than the speed of light in a vacuum. The values of the projections of V_r are also positive along the entire inner boundary of the capillary and have values that are approximately two orders of magnitude smaller than the speed of light in a vacuum. The losses at a wavelength of $1.06 \mu\text{m}$ were 12 dB/m. Thus, the local energy velocity for the fundamental air-core mode is determined at the boundary of the capillary core by fairly simple relations, and the radiation localization in its core is determined by the well-known ARROW model.

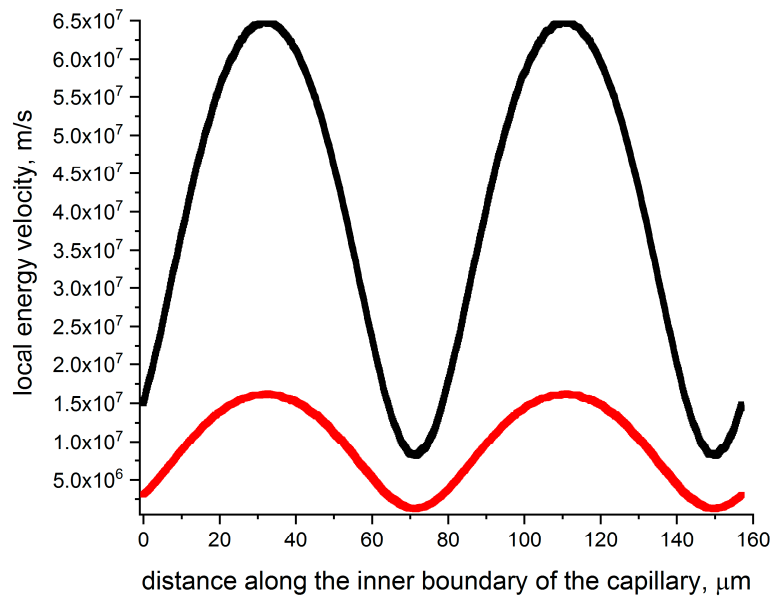


Figure 1. Distribution of axial V_z (black) and radial V_r (red) projections of the local energy velocity for the fundamental air-core mode along the inner boundary of a silica glass capillary with $D_{core} = 50 \mu\text{m}$ and the wall thickness of $t = 750 \text{ nm}$ at $\lambda = 1.06 \mu\text{m}$.

3. Local Energy Velocity of the Fundamental Air-Core Mode for Silica Glass Hollow-Core Fibers with a Negative Curvature of the Core-Cladding Boundary

In this section, we consider the behavior of the local energy velocity of the fundamental air-core mode for two types of silica glass hollow-core fibers shown in Figure 2. The design of such hollow-core fibers is quite simple. A set of silica glass capillaries is placed on a silica glass supporting tube. To demonstrate the behavior of the projections of \vec{V} for the fibers shown in Figure 2, it is sufficient to determine the distribution of the local energy velocity for the fundamental air-core mode (HE_{11} hybrid mode) at the outer boundary of one of the cladding capillaries. The distribution is very similar for all the cladding capillaries.

The first of these (Figure 2a) is a hollow-core fiber with a negative curvature of the core-cladding boundary and an air-core diameter of $D_{core} = 50 \mu\text{m}$, a cladding capillary wall thickness of $t = 750 \text{ nm}$, and an outer diameter of the cladding capillary of $d_{out} = 24 \mu\text{m}$. The second is the well-known nested hollow-core fiber, which is considered the hollow-core fiber with real prospects for applications in telecommunications [7]. Its geometric parameters are an air-core diameter of $D_{core} = 44 \mu\text{m}$, a capillary wall thickness of $t = 490 \text{ nm}$, and an outer diameter of the cladding capillary of $d_{out} = 37.6 \mu\text{m}$, with the

outer diameter of the inner capillary being exactly half of the cladding capillary diameter. The wall thickness of the inner capillary is the same as that of the outer cladding capillary. All numerical calculations in this section were performed using Comsol.

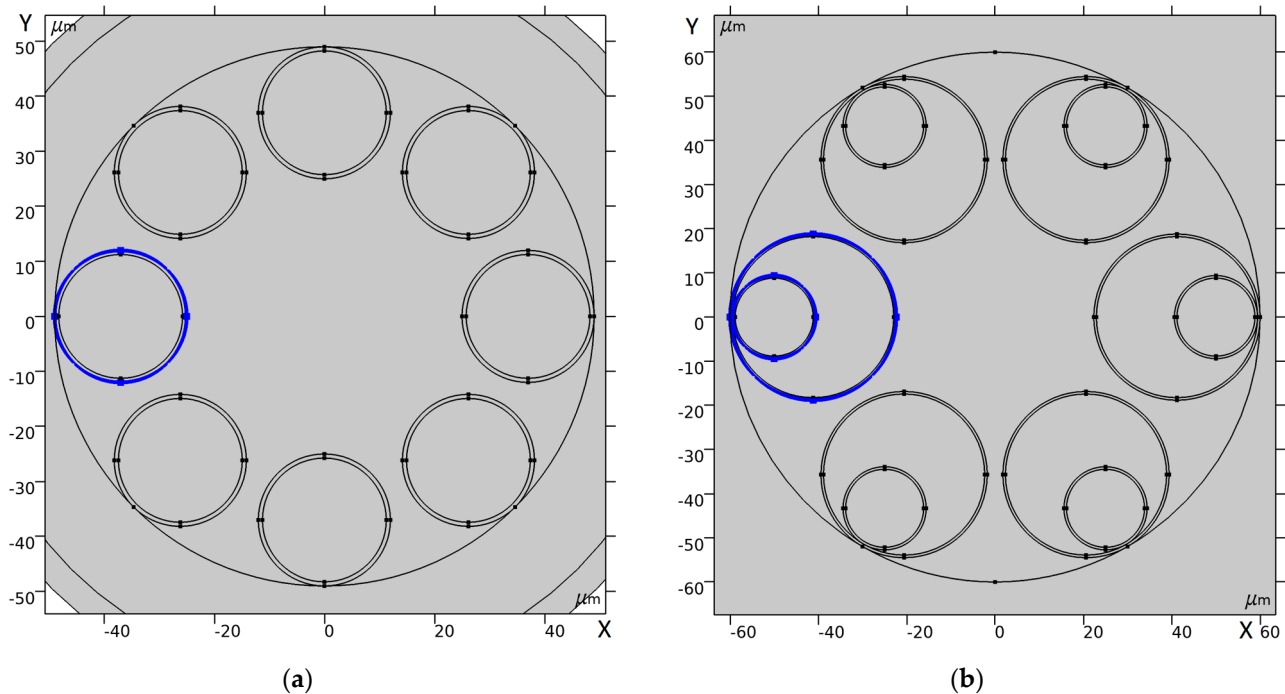


Figure 2. Two hollow-core fibers with a negative curvature of the core-cladding boundary made of silica glass with geometrical parameters described in the text: (a) hollow-core fiber with a cladding consisting of eight capillaries; (b) nested hollow-core fiber with very low losses at a wavelength of 1.55 μm. The blue color indicates the outer boundaries of the cladding capillaries, along which the local energy velocity distribution is considered.

Let us calculate the distribution of projections of V_z and V_r of the local energy velocity (3) for the fundamental air-core mode of the hollow-core fiber shown in Figure 2a. The wavelength is 1.06 μm, which means that, according to the ARROW model, it corresponds approximately to the center of the second transmission band. The distribution of the axial and radial projections of the local energy velocity of the fundamental air-core mode along the outer boundary of the cladding capillary highlighted in blue in Figure 2a is shown in Figure 3. Here it should be said that in this work we simply demonstrate the effects associated with the behavior of the local energy velocity of the fundamental air-core mode of the hollow fibers and the formation of singularities in the Poynting vector of this mode. In our opinion, a more detailed discussion of the behavior of the local energy velocity in the air-core modes depending on the geometrical parameters of hollow-core fibers should be transferred to subsequent works due to the large amount of calculations.

Figure 3 shows that the distribution of the local values of the energy velocity of the fundamental air-core mode at the core-cladding boundary with a negative curvature is qualitatively different from the case of the silica glass capillary considered above (Figure 1). To make this difference even more noticeable, we depicted the same dependencies as in Figure 3, but on a smaller section of the outer boundary of the cladding capillary (along the abscissa). These distributions are shown in Figure 4.

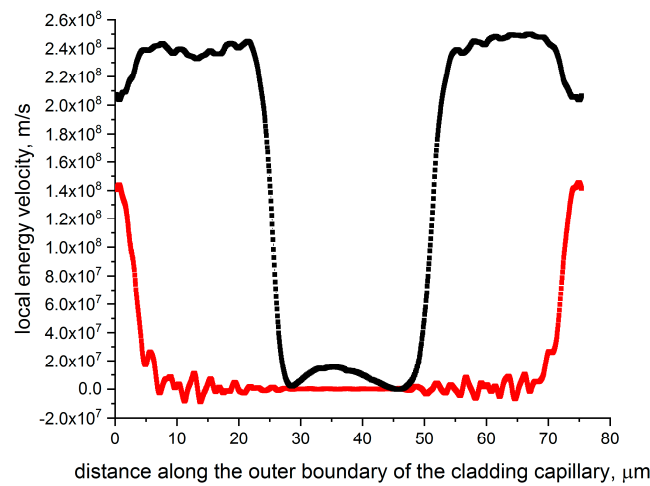


Figure 3. Distribution of axial V_z (black) and radial V_r (red) projections of the local energy velocity for the fundamental air-core mode along the outer boundary of a silica glass cladding capillary for the hollow-core fiber shown in Figure 2a in blue at $\lambda = 1.06 \mu\text{m}$. The distance along the abscissa axis is measured from the place where the capillary is attached to the wall of the supporting tube.

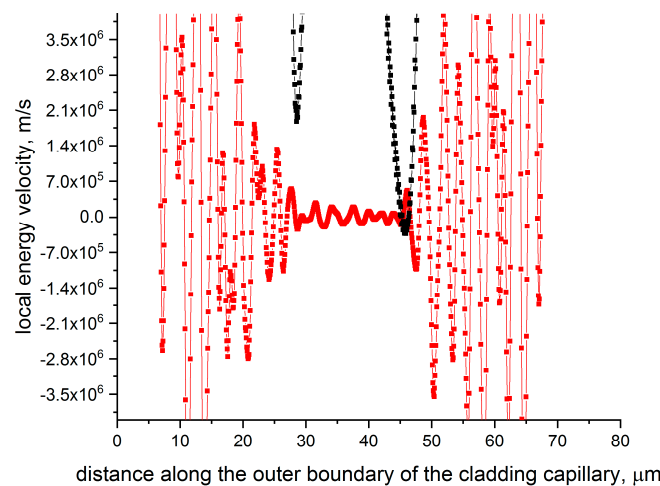


Figure 4. The same distribution of axial V_z (black) and radial V_r (red) projections of the local energy velocity for the fundamental air-core mode along the outer boundary of a silica glass cladding capillary as in Figure 3 but on a smaller section of the outer boundary.

In Figures 3 and 4, the lowest values of the local energy velocity of the fundamental air-core mode are located on the part of the outer boundary of the cladding capillary closest to the center of the hollow-core fiber. Here, the radial projection of V_r of the local energy velocity is of the order of 10^4 m/s and is sign-alternating when passing through zero values. At the same time, the greatest increase in the values of the radial projection of the local energy velocity is in the area of the cladding capillary attachment to the supporting tube (Figures 2 and 3). It should be noted that the loss of the fundamental air-core mode at a wavelength of $\lambda = 1.06 \mu\text{m}$ is 1.2 dB/km . This is almost four orders of magnitude less than the losses for an individual capillary considered in the previous section. Obviously, in the case of the hollow-core fiber shown in Figure 2a, the energy flow of the fundamental air-core mode performs complex motions in the various regions of the cladding capillary wall. This, among other things, leads to a significant decrease in the rate of the air-core mode energy movement in the region of the capillary wall closest to the fiber center (Figure 3). There is even a reverse flow of the air-core mode energy along the z-axis (Figure 4). We will consider the issues related to this movement of the air-core mode of energy in a future publication.

Let us consider in more detail the behavior of the radial projection of V_r of the fundamental air-core mode and, correspondingly, the behavior of the radial projections of the Poynting vector (3). It is clear that the locations of the capillary wall regions where V_r changes its sign should correlate with the locations of the points of the capillary cross-section where the vortex motions of the transverse component of the Poynting vector of the air-core mode occur. The positions of singularities in the transverse component of the Poynting vector $\vec{P}_{transv} = (P_r, P_\phi)$ of the fundamental air-core mode in the cladding capillary wall are determined by the equation of $P_r(x, y) = P_\phi(x, y) = 0$, since the streamlines of the transverse component are determined by the following equation:

$$\frac{dr}{P_r} = \frac{d\phi}{P_\phi}. \tag{5}$$

The corresponding curves are shown in Figure 5 in blue and red for the cladding capillary discussed above (Figure 2a). Figure 5 shows that the curves $P_r(x, y) = P_\phi(x, y) = 0$ have a more ordered and periodic structure in the region of the cladding capillary wall closest to the center of the hollow-core fiber. The structure of the curves is not ordered and disappears in the region where the cladding capillary is attached to the supporting tube. Thus, in the regions of the cladding capillary wall where there is an ordered distribution of singularities of the transverse component of the Poynting vector of the fundamental air-core mode, the local energy velocity of the mode reaches the minimum values and, therefore, leads to the minimum leakage of the air-core mode energy. In the regions of the cladding capillary wall where there is no such structure of singularities of the Poynting vector, the radial projection of the local energy velocity and the outflow of the air-core mode energy are maximal.

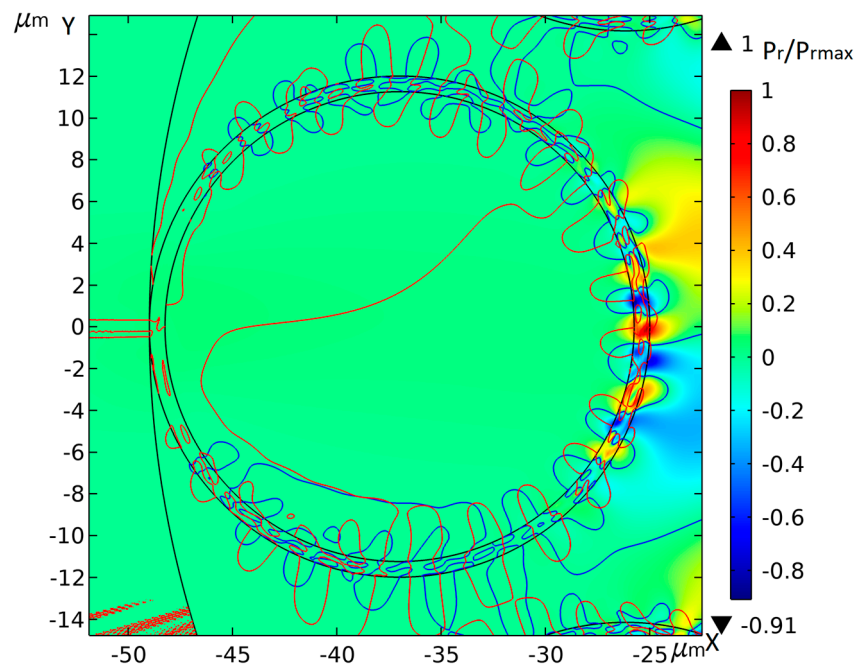


Figure 5. Zero level curves $P_r(x, y) = 0$ (blue) and $P_\phi(x, y) = 0$ (red) for the fundamental air-core mode in the cladding capillary wall. The figure also shows the distribution of the radial projection of the Poynting vector of the fundamental air-core mode; the color bar to the right of the figure shows the normalized value of this projection (its ratio to the maximum value of the radial projection of the Poynting vector in the fiber cross section).

This effect can be greatly enhanced for nested hollow-core fibers (Figure 2b). Let us consider the analogous behavior of the local energy velocity of the fundamental air-core mode at the cladding capillary boundaries of the nested hollow-core fiber (Figure 2b). The

distribution of V_z and V_r will be examined for two wavelengths of 1.55 μm and 2.7 μm in the longest wavelength transmission band. The air-core mode losses at these wavelengths are 0.05 dB/km and 5.7 dB/km, respectively. The distribution of the axial V_z and radial V_r projections of the local energy velocity of the fundamental air-core mode at the outer boundary of the large cladding capillary at a wavelength of 1.55 μm is shown in Figure 6.

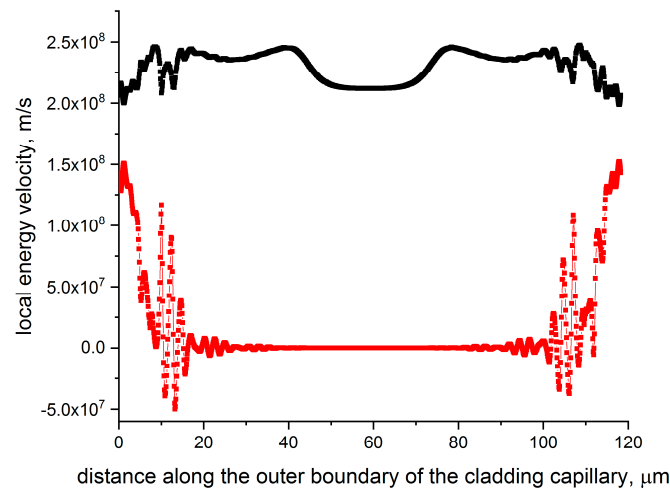


Figure 6. Distribution of axial V_z (black) and radial V_r (red) projections of the local energy velocity for the fundamental air-core mode along the outer boundary of a large silica glass cladding capillary for the nested hollow-core fiber shown in Figure 2b in blue at $\lambda = 1.55 \mu\text{m}$. The distance along the abscissa axis is measured from the place where the capillary is attached to the wall of the supporting tube.

As we can see from Figure 6, the segment of the boundary of the big cladding capillary wall in which the radial projection of the local energy velocity V_r falls comes close to the region where the cladding capillary is attached to the supporting tube. In this case, V_r decreases on average up to 10^4 m/s in the region nearest to the center of the nested hollow-core fiber. The corresponding distribution of the curves $P_r(x, y) = P_\varphi(x, y) = 0$ in the large cladding capillary wall for the fundamental air-core mode is shown in Figure 7.

It can be seen in Figure 7 that there is an ordered distribution of singularities of the transverse component of the Poynting vector of the fundamental air-core mode along virtually the entire wall of large and small cladding capillaries. This correlates well with the position of the large cladding capillary wall region, in which the radial projection of the local energy velocity decreases (Figure 6) and, as a result, the outflow of the fundamental air-core mode energy decreases. The axial projection of the local energy velocity does not have negative values in the case of small losses in the nested hollow-core fiber (Figure 6). It can be demonstrated that similar behavior of V_z and V_r is also observed for a small cladding capillary in the nested hollow-core fiber.

To better demonstrate the alternating behavior dynamics of the radial projection of the local energy velocity of the fundamental air-core mode on the outer boundaries of the small and large cladding capillaries (Figure 2b), we showed the distribution of V_r in the same segment of the outer boundary of both cladding capillaries (Figure 8). Counting in the negative and positive directions was carried out for the cladding capillaries marked in blue in Figure 2b from the $y\text{-axis} = 0$. Figure 8 shows that the radial projection of the local energy velocity oscillates with strict periodicity along the outer boundaries of both cladding capillaries and has zero values for the same values of the azimuthal angle. In addition, the amplitude value of the radial projection of V_r increases by about one order of magnitude at the outer boundary of the small cladding capillary. It can also be seen that by averaging the values of V_r along the given segment of the outer boundaries of both cladding capillaries, we obtain a value close to zero. This means that the power flow of the fundamental air-core mode is blocked in the radial direction in this segment of the cladding capillary boundaries, in the same way as in planar waveguides made of metamaterials [16].

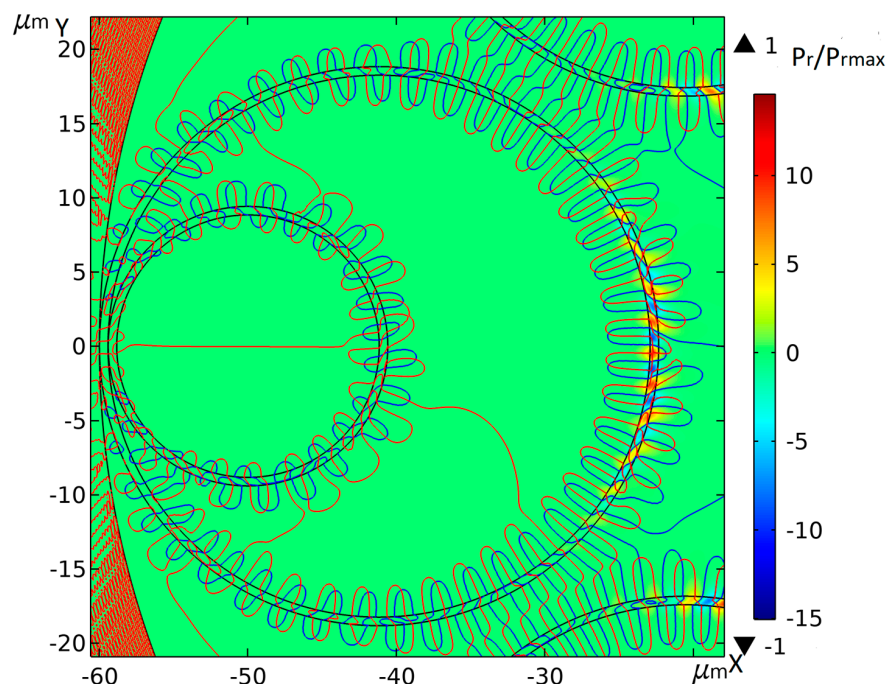


Figure 7. Zero level curves $P_r(x, y) = 0$ (blue) and $P_\phi(x, y) = 0$ (red) for the fundamental air-core mode in the cladding capillary walls of the nested hollow-core fiber (Figure 2b) at a wavelength of $1.55 \mu\text{m}$ and losses of 0.05 dB/km . The figure also shows the distribution of the radial projection of the Poynting vector of the fundamental air-core mode; the color bar to the right of the figure shows the normalized value of this projection (its ratio to the maximum value of the radial projection of the Poynting vector in the fiber cross section).

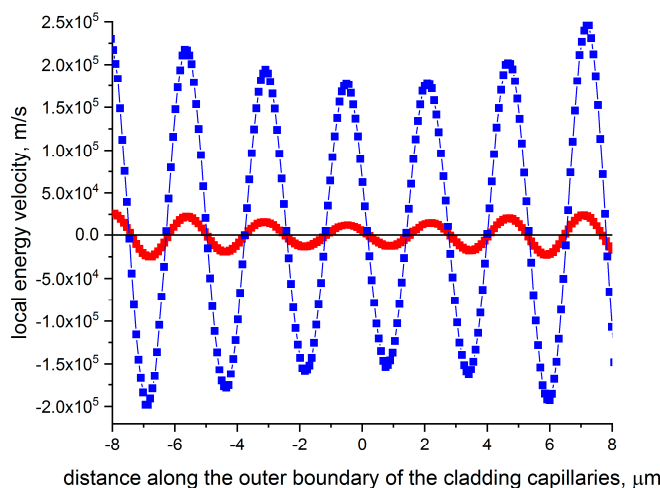


Figure 8. Distribution of the radial projection V_r of the local energy velocity of the fundamental air-core mode along the same segment of the outer boundaries of small (blue) and large (red) cladding capillaries marked in blue in Figure 2b. Counting in the negative and positive directions was carried out from the $y\text{-axis} = 0$ (Figure 2b).

In conclusion, let us consider the behavior of the local energy velocity of the fundamental air-core mode of the nested hollow-core fiber and its distribution of the transverse component of the Poynting vector in the case of an increase in the losses in the longest wavelength transmission band at a wavelength of $2.7 \mu\text{m}$. The distribution of the axial V_z and radial V_r projections of the local energy velocity of the fundamental air-core mode at the outer boundaries of a large cladding capillary at a wavelength of $2.7 \mu\text{m}$ is shown in Figure 9.

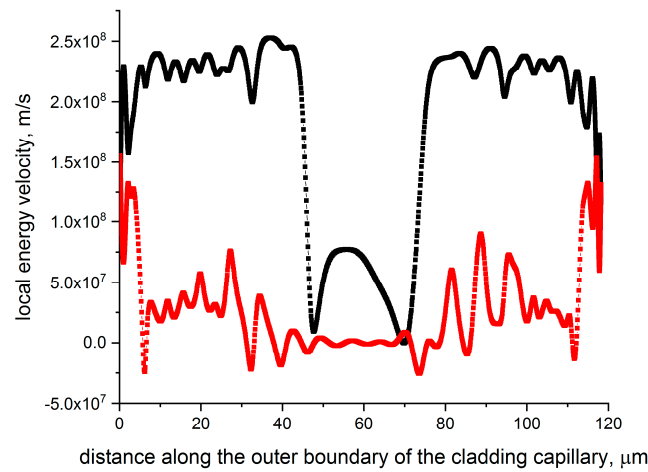


Figure 9. Distribution of axial V_z (black) and radial V_r (red) projections of the local energy velocity for the fundamental air-core mode along the outer boundary of a large silica glass cladding capillary for the nested hollow-core fiber shown in Figure 2b in blue at $\lambda = 2.7 \mu\text{m}$. The distance along the abscissa axis is measured from the place where the capillary is attached to the wall of the supporting tube.

The projection distribution of the local energy velocity of the fundamental air-core mode of a nested hollow-core fiber at increased losses is qualitatively similar to the distribution of these projections for a hollow-core fiber with a cladding consisting of eight capillaries (Figure 3). Oscillations of the values of the radial projections of the local energy velocity with a large amplitude occur along a much larger segment of the cladding capillary wall than in the case of small losses (Figure 6). In addition, the segment of the capillary wall on which a significant decrease in the radial projection of the local energy velocity occurs is much smaller than in the case of small losses. All this suggests that a significant rearrangement of the structure of the singularities of the transverse component of the Poynting vector of the fundamental air-core mode should take place. This can be seen in Figure 10.

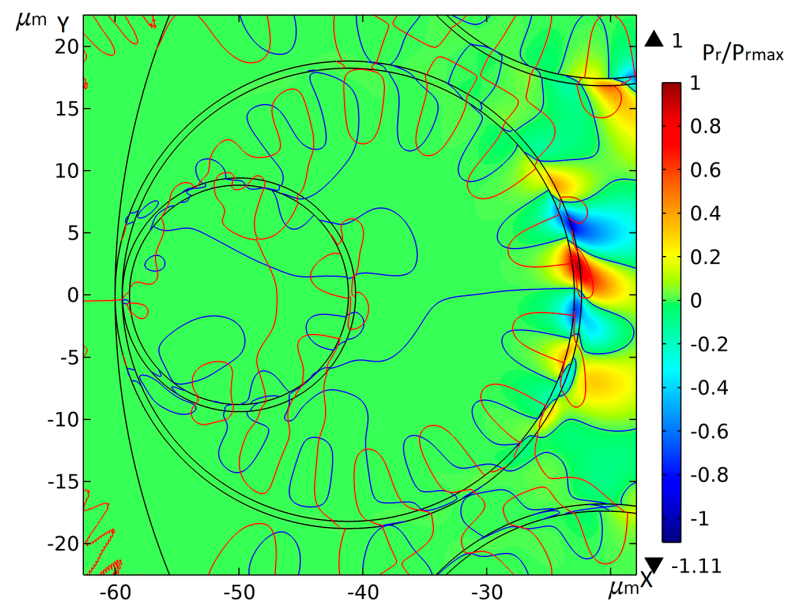


Figure 10. Zero level curves $P_r(x, y) = 0$ (blue) and $P_\phi(x, y) = 0$ (red) for the fundamental air-core mode in the cladding capillary walls of the nested hollow-core fiber (Figure 2b) at a wavelength of $2.7 \mu\text{m}$ and losses of 5.7 dB/km . The figure also shows the distribution of the radial projection of the Poynting vector of the fundamental air-core mode; the color bar to the right of the figure shows the normalized value of this projection (its ratio to the maximum value of the radial projection of the Poynting vector in the fiber cross section).

The number of singularities in the transverse component of the Poynting vector of the fundamental air-core mode along the capillary wall has significantly decreased, and so did the order of their arrangement. The periodicity of the arrangement of singularities on a small capillary wall, observed for small losses, has, in fact, disappeared. All this points to a direct connection between the occurrence and location of the singularities of the Poynting vector of the air-core mode and the behavior of leakage losses in hollow-core fibers.

4. Discussion

In this paper, we have considered two types of hollow-core fibers most commonly used, namely, a single silica glass capillary and a hollow-core fiber with a negative curvature of the core-cladding boundary. Until recently, there have been extensive discussions about which model best describes light localization in the second type of hollow-core fibers. In the case of light localization in a glass capillary, the situation is quite clear, since the radial projection of the Poynting vector P_r of the fundamental air-core mode does not change sign in the capillary wall, the $P_r(x, y) = P_\phi(x, y) = 0$ curves do not intersect each other, and they do not wind along the core-cladding boundary. In this case, we can say that the ARROW model proposed for planar waveguides, to a good approximation, describes the process of antiresonant reflection from the capillary wall despite its curved boundary. This is especially true for capillaries with large core diameters compared to the wavelength. The local energy velocity of the air-core mode can be expressed analytically and has a periodic distribution along the azimuthal direction. Its radial projection of V_r has values approximately an order of magnitude smaller than the axial projection of V_z . In addition, as mentioned above, the radial projection has positive values along the entire wall of a single capillary. Therefore, the leakage losses in the silica glass capillary are always high in the near and mid-IR spectral ranges. Thus, the curvature of the core-cladding boundary in the case of a silica glass capillary plays an implicit role, and the degree of light localization in the air core is determined mainly by the capillary wall thickness and its ratio with the wavelength used in each case.

However, a hollow-core fiber with a negative curvature of the core-cladding boundary manifests a very different behavior. In this case, the values of the radial projection of the local energy velocity of the fundamental air-core mode drop by several orders of magnitude compared to the speed of light in air over most of the cladding capillary wall boundary. In addition, it periodically vanishes and changes signs along the cladding capillary wall. The air-core mode energy does not move in the radial direction at points with zero values of the radial projection of the local energy velocity. This happens because singularities of the transverse component of the Poynting vector of the fundamental air-core mode appear along the cladding capillary wall, in the vicinity of which the power flow of the air-core mode has both positive and negative values in the radial direction. This leads to a mutual cancellation of the power flows of the air-core mode in the singularity region. Similar areas of singularities for the transverse component of the Poynting vector of the fundamental air-core mode are also observed between the cladding capillaries, which leads to additional blocking of the air-core mode energy in the air-core of the hollow-core fiber and to a further decrease in its losses. As already mentioned in the Introduction, similar phenomena occur in a planar sandwich waveguide structure consisting of epsilon-negative/left-handed/epsilon-negative metamaterials when the power flows of vortex-guided mode are cancelled almost totally between the core and the cladding.

In conclusion, we would like to hope that the ideas expressed in this work can help to better understand the mechanism of radiation leakage in hollow-core fibers with a complex shape of the core-cladding boundary. It is possible that the study of the relationship between the geometric parameters of the hollow-core fibers and the process of formation of sets of singularities in the Poynting vector of the air-core modes will lead to an understanding of how to further reduce losses in hollow-core fibers.

Funding: This research was funded by the Russian Science Foundation, grant number 22-22-00575.

Institutional Review Board Statement: Not applicable.

Informed Consent Statement: Not applicable.

Data Availability Statement: The data that support the findings of this study are available upon request from the corresponding author.

Conflicts of Interest: The author declares no conflict of interest.

References

1. Marcatili, E.A.J.; Schmeltzer, R.A. Hollow metallic and dielectric waveguides for long distance optical transmission and lasers. *Bell. Syst. Tech. J.* **1964**, *43*, 1783–1809. [[CrossRef](#)]
2. Russell, P.S.J. Photonic-crystal fibers. *J. Light. Technol.* **2006**, *24*, 4729–4749. [[CrossRef](#)]
3. Roberts, P.J.; Couny, F.; Sabert, H.; Mangan, B.J.; Williams, D.P.; Farr, L.; Mason, M.W.; Tomlinson, A.; Birks, T.A.; Knight, J.C.; et al. Ultimate low loss of hollow-core photonic crystal fibres. *Opt. Express* **2005**, *13*, 236–244. [[CrossRef](#)] [[PubMed](#)]
4. Pryamikov, A.D.; Biriukov, A.S.; Kosolapov, A.F.; Plotnichenko, V.G.; Semjonov, S.L.; Dianov, E.M. Demonstration of a waveguide regime for a silica hollow-core microstructured optical fiber with a negative curvature of the core cladding boundary in the spectral region $> 3.5 \mu\text{m}$. *Opt. Express* **2011**, *19*, 1441–1448. [[CrossRef](#)] [[PubMed](#)]
5. Wang, Y.Y.; Wheeler, N.V.; Couny, F.; Roberts, P.J.; Benabid, F. Low loss broadband transmission in hypocycloid-core Kagome hollow-core photonic crystal fiber. *Opt. Lett.* **2011**, *36*, 669–671. [[CrossRef](#)] [[PubMed](#)]
6. Yu, F.; Wadsworth, J.; Knight, J.C. Low loss silica hollow core fibers for 3–4 μm spectral region. *Opt. Express* **2012**, *20*, 11153–11158. [[CrossRef](#)] [[PubMed](#)]
7. Fokoua, E.N.; Mousavi, S.A.; Jasion, G.T.; Richardson, D.J.; Poletti, F. Loss in hollow-core optical fibers: Mechanisms, scaling rules, and limits. *Adv. Opt. Photonics* **2023**, *15*, 1–85. [[CrossRef](#)]
8. Kolyadin, A.N.; Kosolapov, A.F.; Pryamikov, A.D.; Biriukov, A.S.; Plotnichenko, V.G.; Dianov, E.M. Light transmission in negative curvature hollow core fiber in extremely high material loss region. *Opt. Express* **2013**, *21*, 9514–9519. [[CrossRef](#)] [[PubMed](#)]
9. Bufetov, I.A.; Kolyadin, A.N.; Kosolapov, A.F.; Efremov, V.P.; Fortov, V.E. Catastrophic damage in hollow core optical fibers under high power laser radiation. *Opt. Express* **2019**, *27*, 18296–18310. [[CrossRef](#)]
10. Litchinitser, N.M.; Abeeluck, A.K.; Headley, C.; Eggleton, B.J. Antiresonant reflecting photonic crystal optical waveguides. *Opt. Lett.* **2002**, *27*, 1592–1594. [[CrossRef](#)] [[PubMed](#)]
11. Poletti, F. Nested antiresonant nodeless hollow core fiber. *Opt. Express* **2014**, *22*, 23807–23828. [[CrossRef](#)] [[PubMed](#)]
12. Debord, B.; Amsanpally, M.; Chafer, M.; Baz, A.; Maurel, M.; Blondy, J.M.; Hugonnot, E.; Scol, F.; Vincetti, L.; Gerome, F.; et al. Ultralow transmission loss in inhibited-coupling guiding hollow fibers. *Optica* **2017**, *4*, 209–217. [[CrossRef](#)]
13. Pryamikov, A.; Alagashev, G.; Falkovich, G.; Turitsyn, S. Light transport and vortex-supported wave-guiding in micro-structured optical fibres. *Sci. Rep.* **2020**, *10*, 2507. [[CrossRef](#)] [[PubMed](#)]
14. Murphy, L.R.; Bird, D. Azimuthal confinement: The missing ingredient in understanding confinement loss in antiresonant, hollow-core fibers. *Optica* **2023**, *10*, 854–870. [[CrossRef](#)]
15. Webb, K.J.; Yang, M.-C. Generation and control of optical vortices using left-handed materials. *Phys. Rev. E* **2006**, *74*, 016601. [[CrossRef](#)] [[PubMed](#)]
16. Dong, J.W.; Wang, H.Z. Slow electromagnetic propagation with low group velocity dispersion in an all-metamaterial-based waveguide. *Appl. Phys. Lett.* **2007**, *91*, 111909. [[CrossRef](#)]
17. Shevchenko, V.V. Forward and backward waves: Three definitions and their correlation and applicability. *Physics-Uspokhi* **2007**, *50*, 287–292. [[CrossRef](#)]
18. Pryamikov, A.D.; Alagashev, G.K. Strong light localization and a peculiar feature of light leakage in the negative curvature hollow core fibers. *Fibers* **2017**, *5*, 43. [[CrossRef](#)]
19. Pryamikov, A.D.; Alagashev, G.K. Features of light leakage from the negative curvature hollow core fibers. *Opt. Eng.* **2018**, *57*, 066106. [[CrossRef](#)]
20. Pryamikov, A.D. Phase dislocations in hollow core waveguides. *Fibers* **2021**, *9*, 59. [[CrossRef](#)]

Disclaimer/Publisher’s Note: The statements, opinions and data contained in all publications are solely those of the individual author(s) and contributor(s) and not of MDPI and/or the editor(s). MDPI and/or the editor(s) disclaim responsibility for any injury to people or property resulting from any ideas, methods, instructions or products referred to in the content.